

# Ultrafast phonon-driven charge transfer in van der Waals heterostructures

Giuseppe Meneghini,<sup>1,\*</sup> Samuel Brem,<sup>1</sup> and Ermin Malic<sup>1,2</sup>

<sup>1</sup>*Department of Physics, Philipps University of Marburg, 35037 Marburg, Germany*

<sup>2</sup>*Department of Physics, Chalmers University of Technology, 41258 Göteborg, Sweden*

(Dated: September 9, 2022)

Van der Waals heterostructures built by vertically stacked transition metal dichalcogenides (TMDs) exhibit a rich energy landscape including interlayer and intervalley excitons. Recent experiments demonstrated an ultrafast charge transfer in TMD heterostructures. However, the nature of the charge transfer process has remained elusive. Based on a microscopic and material-realistic exciton theory, we reveal that phonon-mediated scattering via strongly hybridized intervalley excitons governs the charge transfer process that occurs on a sub-100fs timescale. We track the time-, momentum-, and energy-resolved relaxation dynamics of optically excited excitons and determine the temperature- and stacking-dependent charge transfer time for different TMD bilayers. The provided insights present a major step in microscopic understanding of the technologically important charge transfer process in van der Waals heterostructures.

Transition-metal dichalcogenides (TMDs) have been in the focus of current research due to their enhanced light-matter and Coulomb interaction leading to a rich energy landscape of tightly bound excitons [1–4]. Stacking TMD monolayers into van der Waals heterostructures introduces spatially separated interlayer states adding another exciton species with long lifetimes and an out-of-plane dipole moment [5–14]. Recent experiments demonstrated the ultrafast charge transfer in optically excited TMD heterobilayers resulting in a formation of interlayer states on a sub-picosecond timescale [15–20]. Typically, TMD heterobilayers exhibit a type-II band alignment [21, 22] favoring the tunneling of an electron or hole into the opposite layer. However, the underlying microscopic nature of the charge transfer process has not yet been well understood. In an early previous work, we have suggested a defect-assisted interlayer tunneling directly at the K point [18, 23]. Alternatively, a phonon-mediated charge transfer could occur involving intervalley scattering to the strongly hybridized  $\Lambda$  or  $\Gamma$  valleys [24–26]. A sophisticated microscopic model of such a phonon-assisted formation of interlayer excitons is still missing.

In this work, we address this open question and reveal the crucial many-particle mechanism behind the ultrafast charge transfer in TMD heterostructures. To this end, we combine first-principle calculations [27] with the excitonic density matrix formalism [28, 29] to obtain a material-realistic model of the excitonic energy landscape, the internal substructure of different exciton species and the phonon-mediated scattering into layer-hybridized dark intervalley states [30, 31]. We first calculate the exciton energy landscape of the exemplary  $\text{MoS}_2\text{-WS}_2$  and  $\text{MoSe}_2\text{-WSe}_2$  heterostructures by solving the Wannier equation for perfectly layer-polarized intra- and interlayer excitons and subsequently computing hybrid excitons based on first-principle interlayer tunneling parameters [18, 23, 28, 30, 31]. Then, we develop and numerically solve equations of motion describing the time- and momentum-resolved evolution of hybrid ex-

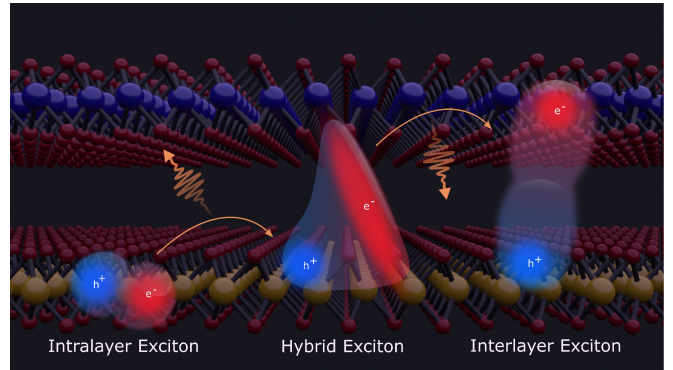


FIG. 1. Sketch of the charge transfer process. Starting from an exciton localized in the bottom layer, phonon-mediated scattering to an hybrid exciton state (where e.g. the electron lives in both layers) allows for the transfer of the charge (here electron) to the upper layer resulting in a spatially separated interlayer exciton state. In analogy, hole transfer can also take place if hybrid excitons with delocalized holes are present.

citons. This allows us to track the relaxation dynamics of excitons from optically excited intralayer excitons towards charge separated interlayer exciton states. We identify the phonon-mediated intervalley scattering from intralayer  $\text{KK}$  into the strongly hybridized  $\text{KA}'$  excitons, followed by the relaxation into energetically lower interlayer  $\text{KK}^{(\prime)}$  states, as the crucial mechanism behind the ultrafast charge transfer in these heterostructures, cf. Fig 1. We further determine the characteristic temperature- and stacking-dependent charge transfer time that can guide future experiments investigating interlayer excitons in van der Waals heterostructures.

*Microscopic approach:* The starting point of this work is the Hamilton operator describing electrons and holes of the heterostructure in the basis of monolayer eigenstates (localized in one of both layers). Here we include a stacking-dependent alignment shift of the two monolayer band structures [32] as well as interlayer tunneling

terms resulting from the wave function overlap between the adjacent layers. The necessary material-specific parameters have been extracted from first-principle calculations [27]. Moreover, we include many-particle interaction Hamiltonians, such as electron-light and electron-phonon coupling as well as the Coulomb interaction between electrons and holes. Here, the scattering between electrons and photons/phonons preferably occurs locally within one of the two layers, whereas we explicitly include the Coulomb interaction between particles residing in different layers. The different intra- and interlayer Coulomb matrix elements are computed with a modified Keldysh-type potential [23, 28, 30] accounting for the dielectric environment created by the TMD layers and the substrate [33]. To achieve a numerically feasible model we set the twist-angle between the two monolayers to zero and study the charge transfer in a spatially homogeneous system characterized by a single atomic alignment. Although the twist-angle is known to have a large impact on the hybridization of exciton states [30], we expect the qualitative charge transfer behaviour to remain the same also in twisted heterostructures. Moreover, we do not consider spin-flipping processes and restrict our model to the optically active (A exciton) spin configuration, as the spin-flipping processes are expected to occur on a slower timescale [34, 35].

Now, we derive the dynamics of the system by initially performing a series of basis transformations. First we solve the Wannier equation for pure intra- or inter-layer excitons [23] and use the eigenfunctions  $\psi^\mu(\mathbf{k})$  to introduce a new set of excitonic operators [30]  $X_{\mathbf{Q}}^{\mu\dagger} = \sum_{\mathbf{k}} \psi^\mu(\mathbf{k}) a_{c,\zeta_e,L_e,\mathbf{k}+\alpha\mathbf{Q}}^\dagger a_{v,\zeta_h,L_h,\mathbf{k}-\beta\mathbf{Q}}$  with the compound quantum number  $\mu = (n, \zeta, L)$  labelling the excitonic states. Here  $n$  is associated to the series of Rydberg-like states determining the relative electron-hole motion,  $\zeta = (\zeta_e, \zeta_h)$  denotes the electron and hole valleys and the layer compound index  $L = (L_e, L_h)$  contains the electron and hole layer. Furthermore, we have introduced the center-of-mass momentum  $\mathbf{Q}$  and the relative momentum  $\mathbf{k}$  between electrons and holes. The operator  $a_i^{(\dagger)}$  is annihilating (creating) electrons with the set of quantum numbers denoted by  $i$ . We use the new exciton operators to perform a basis transformation to obtain an effective single-particle Hamiltonian for excitons, reading

$$H_X = \sum_{\mu\mathbf{Q}} E_{\mathbf{Q}}^\mu X_{\mathbf{Q}}^{\mu\dagger} X_{\mathbf{Q}}^\mu + \sum_{\mu\nu\mathbf{Q}} \mathcal{T}_{\mu\nu} X_{\mathbf{Q}}^{\mu\dagger} X_{\mathbf{Q}}^\nu \quad (1)$$

with the exciton energy  $E_{\mathbf{Q}}^\mu$  obtained from the Wannier equation and the excitonic tunnelling matrix elements  $\mathcal{T}_{\mu\nu}$ , which contain apart from electronic tunneling rates also the overlap of excitonic wave functions.

Next, we diagonalize the exciton Hamiltonian Eq. 1 by introducing a new set of operators  $Y_{\mathbf{Q}}^\eta = \sum_{\mu} c_\mu^\eta(\mathbf{Q}) X_{\mathbf{Q}}^\mu$  describing hybrid excitons. These are layer-hybridized states consisting of intra- and interlayer excitons with the

mixing coefficients  $c_\mu^\eta(\mathbf{Q})$  and the new quantum number  $\eta$  defining the hybrid-exciton bands. The diagonalized Hamiltonian reads in this basis  $H_Y = \sum_{\eta} \mathcal{E}_{\mathbf{Q}}^\eta Y_{\mathbf{Q}}^{\eta\dagger} Y_{\mathbf{Q}}^\eta$  with the corresponding hybrid-exciton energies  $\mathcal{E}_{\mathbf{Q}}^\eta$ . With the procedure described above we have a microscopic access to the full spectrum of strongly or weakly hybridized exciton states including bright KK as well as momentum-dark intervalley states [36, 37], such as  $\text{K}\Lambda'$  and  $\text{K}\text{K}'$ , cf. Fig. 2 that will be discussed further below.

Finally, we consider the interaction of hybrid exciton states with phonons. As we restrict our study to the low-density regime, exciton-exciton scattering can be neglected [38]. Starting from the electron-hole picture and performing the same change of basis as described above, we obtain the following Hamiltonian for the hybrid-exciton-phonon interaction [30]

$$H_{Y\text{-ph}} = \sum_{\substack{\mathbf{Q}, \mathbf{q}, \\ j, \eta, \xi}} \mathcal{D}_{j\mathbf{q}}^{\xi\eta} Y_{\mathbf{Q}+\mathbf{q}}^{\xi\dagger} Y_{\mathbf{Q}}^\eta b_{j,\mathbf{q}} + h.c. \quad (2)$$

as well as for the hybrid-exciton-light coupling  $H_{Y\text{-l}} = \sum_{\sigma, \mathbf{Q}, \eta} \mathbf{A} \cdot \mathcal{M}_{\sigma\mathbf{Q}}^\eta Y_{\mathbf{Q}}^\eta + h.c.$  All details on the basis transformation and the resulting hybrid matrix elements can be found in the SI.

Having determined the Hamilton operator  $H = H_Y + H_{Y\text{-ph}} + H_{Y\text{-l}}$  for hybrid-excitons and their interaction with phonons and light, we can now derive equations of motion describing the exciton dynamics. Here we exploit the Heisenberg equation of motion for the occupation numbers  $N_{\mathbf{Q}}^\eta = \langle Y_{\mathbf{Q}}^{\eta\dagger} Y_{\mathbf{Q}}^\eta \rangle$ , truncating the Martin-Schwinger hierarchy arising from the exciton phonon-scattering within the second-order Born-Markov approximation [36, 39–41]. Considering separately the coherent polarization  $P_{\mathbf{Q}}^\eta = \langle Y_{\mathbf{Q}}^{\eta\dagger} \rangle$  and the purely incoherent population  $\delta N_{\mathbf{Q}}^\eta = N_{\mathbf{Q}}^\eta - |P_{\mathbf{Q}}^\eta|^2$ , we arrive at the semiconductor Bloch-equations in hybrid-exciton basis

$$i\hbar\dot{P}_0^\eta = -(\mathcal{E}_0^\eta + i\Gamma_0^\eta)P_0^\eta - \mathcal{M}_0^\eta \cdot \mathbf{A}(t) \quad (3)$$

$$\delta\dot{N}_{\mathbf{Q}}^\eta = \sum_{\xi} W_{0\mathbf{Q}}^{\xi\eta} |P_0^\eta|^2 + \sum_{\xi, \mathbf{Q}'} \left( W_{\mathbf{Q}'\mathbf{Q}}^{\xi\eta} \delta N_{\mathbf{Q}'}^\xi - W_{\mathbf{Q}\mathbf{Q}'}^{\eta\xi} \delta N_{\mathbf{Q}}^\eta \right).$$

The details on the scattering tensor  $W_{\mathbf{Q}'\mathbf{Q}}^{\xi\eta}$  can be found in the SI. Equation (3) provides full microscopic access to the dynamics of hybrid excitons including optical excitation as well as phonon-scattering-induced relaxation across intra- and intervalley as well as intra- and inter-layer states, effectively giving rise to a multi-step charge transfer process.

## HYBRID EXCITON LANDSCAPE

We focus here on the two most studied heterostructures in literature,  $\text{MoS}_2\text{-WS}_2$  and  $\text{MoSe}_2\text{-WSe}_2$ . For simplicity, we show the results for the latter in the main text and

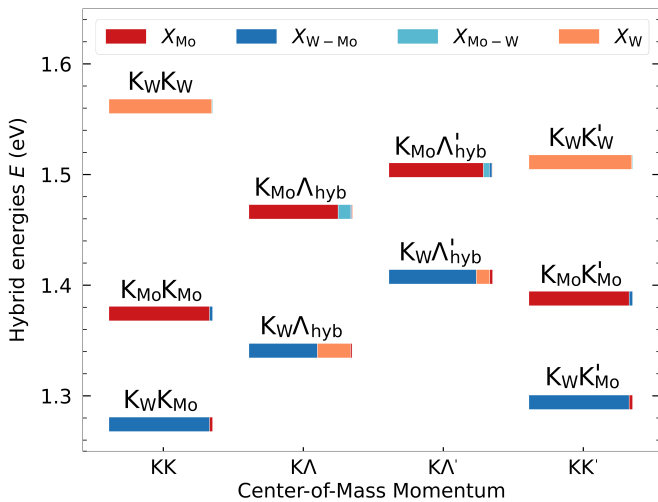


FIG. 2. Hybrid-exciton energy landscape for  $\text{MoSe}_2\text{-WSe}_2$  ( $R_h^h$  stacking). We use different colors for depicting the four initial intra- and interlayer excitonic states named with  $X_{l_h-l_e}$  (using only one index for intralayer excitons). The final hybrid exciton states are denoted with two capital letters (K,  $\Lambda$ ) describing the valley and the subscripts (W, Mo) describing the layer, in which the hole (first letter) and electron (second letter) are localized. We highlight for each hybrid exciton the percentage of the involved intra- and interlayer exciton states. Due to the strong tunneling experienced by electrons, the states in the  $K\Lambda^{(\prime)}$  valleys are strongly hybridized. Note that we plot only a selection of low-energy hybrid exciton states contributing directly to the relaxation dynamics.

the former in the SI. We start by presenting the hybrid exciton landscape that has been calculated by solving the Wannier equation in the hybrid-exciton basis, cf. Fig. 2. This energy landscape is the key to understanding the charge transfer process. We use the following notation for the hybrid exciton states: the capital letters describe the valley and the subscript the layer, where the first letter denotes the hole and the second the electron. To give an example,  $K_W K'_\text{Mo}$  means that the hole is located at the K point of the  $\text{WSe}_2$  layer, while the electron is localized at the  $K'$  valley of the  $\text{MoSe}_2$  layer. Furthermore, we use the subscript *hyb* to underline that the electron/hole in the corresponding valley is strongly hybridised between both layers, e.g. in  $K_W \Lambda_{\text{hyb}}$  the electron at the  $\Lambda$  valley lives in both layers.

Figure 2 shows the energy landscape of hybrid-excitons in the  $\text{MoSe}_2\text{-WSe}_2$  heterostructure for the case of  $R_h^h$  stacking, i.e. the metal atoms of one layer are placed on top of the metal atoms of the other layer. The corresponding landscape for the other two high-symmetry stackings  $R_h^X$  and  $R_h^M$  [27] (where either the chalcogen atom X or the metal atom M of the upper layer is above the hole/void of the other layer) as well as for the  $\text{MoS}_2\text{-WS}_2$  heterostructure can be found in the SI. We show only the hybrid exciton states that are energetically close

to or lower than the intralayer  $K_W K_W$  exciton in the  $\text{WSe}_2$  layer, since we will resonantly excite the material at this exciton energy and phonon-driven relaxation processes will distribute the excitons towards lower energies. We have checked that the contribution of higher exciton states to the relaxation dynamics and the charge transfer process, i.e. due to absorption of phonons, is negligible. Note that for this particular heterostructure  $\Gamma K$  excitons do not play a role for the charge transfer process, while their are crucial for the  $\text{MoS}_2\text{-WS}_2$  heterostructure considered in the SI.

In the exciton basis, the hybridization of electronic states corresponds to a mixing of intra- and interlayer excitons. We quantify the contribution of each state to the new hybrid-exciton states by evaluating the mixing coefficients. Here,  $|c_\mu^\eta(\mathbf{Q})|^2$  can be interpreted as the percentage of the exciton state  $\mu$  inside the hybrid state  $\eta$ . In the presence of strong tunnelling the new hybrid states are expected to be heavily influenced by different excitonic species. In contrast, a weak tunnelling should result in hybrid states that are almost purely intra- or interlayer excitons. The degree of hybridisation of each state is illustrated in Fig. 2 by adopting a color scheme, where we highlight for each hybrid state the different exciton contributions. Here, a hybrid state of a pure intralayer or interlayer character is just red or blue, respectively. In contrast, strongly hybridised states consist of different colors. Figure 2 illustrates that hybrid states involving excitons at the  $\Lambda$  valley ( $K_W \Lambda_{\text{hyb}}$ ,  $K_W \Lambda'_{\text{hyb}}$ ) contain large contributions of several species, whereas the states at the K valley are either intra- or interlayer excitons to a very high percentage. The weak hybridisation of  $KK$  excitons is well known in literature [42, 43]. The electronic wave functions at the K valley are mostly composed of d orbitals localized at transition metal atoms, which are sandwiched by the selenium atoms preventing an efficient overlap of wave functions. In contrast, the electronic wave function at the  $\Lambda$  valley has large contributions at the selenium atoms resulting in much more efficient hybridisation of  $K_W \Lambda_{\text{hyb}}^{(\prime)}$  states [30, 31, 42, 43].

The energetically lowest states in the investigated  $\text{MoSe}_2\text{-WSe}_2$  heterostructure are  $K_W K_{\text{Mo}}^{(\prime)}$  excitons that are almost purely of interlayer exciton character (blue). When exciting the material resonantly to the intralayer  $K_W K_W$  state (orange), there is a number of spectrally lower-lying states that will give rise to a phonon-mediated cascade of transitions down to the energetically lowest states. Note that the scattering process between two hybrid states requires that the initial and final states live at least partially in the same layer. Therefore, we expect the strongly hybridised exciton states  $K_W \Lambda_{\text{hyb}}^{(\prime)}$  to play a major role for the relaxation dynamics and the charge transfer process.

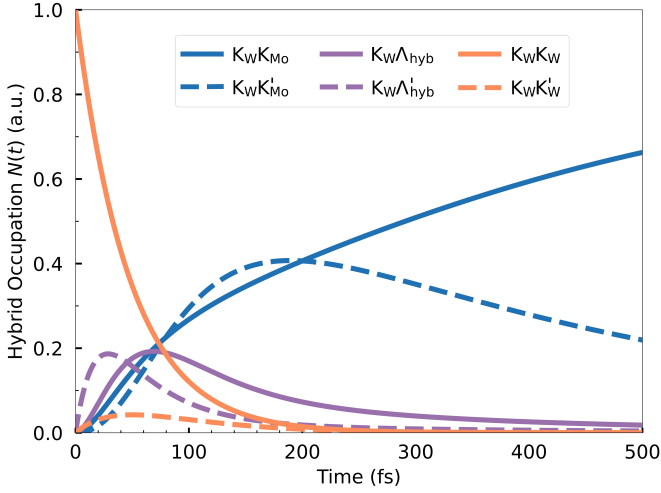


FIG. 3. Momentum-integrated hybrid-exciton dynamics at 77 K for MoSe<sub>2</sub>-WSe<sub>2</sub> in R<sub>h</sub><sup>h</sup> stacking. By solving Eq. (3), we have microscopic access to the phonon-mediated relaxation dynamics of hybrid exciton and the resulting charge transfer mechanism. Starting with an initial occupation of intralayer K<sub>W</sub>K<sub>W</sub> excitons localized in the WSe<sub>2</sub> layer (orange line) via phonon-mediated scattering into the strongly hybridized K<sub>W</sub>Λ<sub>hyb</sub><sup>(l)</sup> states (purple lines), we end up in the energetically lowest interlayer K<sub>W</sub>K<sub>Mo</sub><sup>(l)</sup> excitons (blue lines), i.e. the electron has been transferred to the MoSe<sub>2</sub> layer.

## HYBRID EXCITON DYNAMICS

Now, we investigate the time- and momentum-resolved relaxation cascade of hybrid excitons after an optical excitation resonant to the purely intralayer K<sub>W</sub>K<sub>W</sub> exciton localized in the WSe<sub>2</sub> layer, cf. Fig. 2. To focus on the charge transfer process and to avoid interplay effects with the exciting laser pulse, we directly initialize the system with a population in the K<sub>W</sub>K<sub>W</sub> state. We have also performed calculations including the laser pulse and the interference of optical excitation and relaxation dynamics, which are presented in the SI. Note that we focus on the 1s ground state for all exciton species, as higher-energy states in the Rydberg-like series of excitons exhibit a much smaller scattering probability compared to the 1s-1s transitions [44]. This has been verified by numerically evaluating phonon-assisted scattering involving higher-energy states.

Evaluating the semiconductor Bloch equations (cf. Eq. (3)), we have full microscopic access to the time-, energy- and momentum-resolved relaxation cascade of non-equilibrium excitons. Figure 3 shows the momentum-integrated exciton dynamics in MoSe<sub>2</sub>-WSe<sub>2</sub> (in R<sub>h</sub><sup>h</sup> stacking) at 77 K. We see a decrease of the initially populated intralayer K<sub>W</sub>K<sub>W</sub> exciton state (solid orange line). At the same time, we find an ultrafast increase in the population of the hybrid K<sub>W</sub>Λ<sub>hyb</sub><sup>(l)</sup> excitons on a timescale of sub-100fs (solid and dashed purple

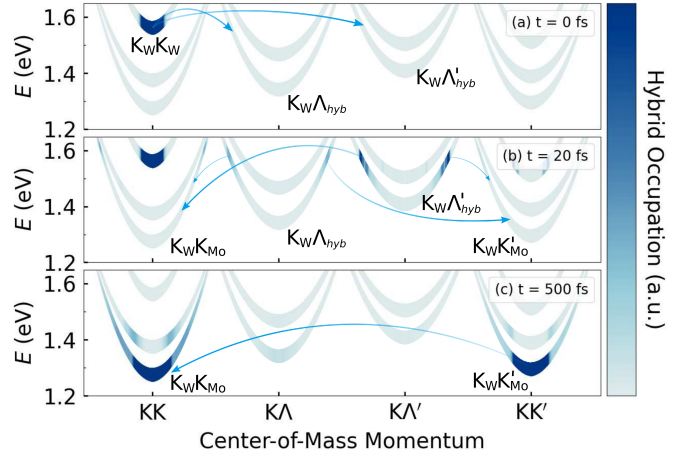


FIG. 4. Momentum-resolved hybrid-exciton dynamics at (a) 0 fs, (b) 20 fs, and (c) 500 fs. Starting from a population created in the intralayer K<sub>W</sub>K<sub>W</sub> exciton, we highlight the most important phonon-driven scattering processes. Note that the blue-shading in the parabolas corresponds to a microscopically calculated exciton occupation. The charge transfer of electrons occurs in a two-step process with an initial partial transfer into the hybrid K<sub>W</sub>Λ<sub>hyb</sub><sup>(l)</sup> exciton states (with the electron living in both layers) followed by the complete transfer to the energetically lower interlayer K<sub>W</sub>K<sub>Mo</sub><sup>(l)</sup> states (with the electron localized in the second layer).

lines). The microscopic origin of this efficient scattering lies in the nature of the hybrid-exciton-phonon coupling. Phonons can only couple states that share the same layer quantum number  $L = (L_e, L_h)$  as exciton-phonon scattering is considered to be a local process. For this reason, phonons can couple pure intra- and interlayer states only through scattering via hybrid states. Once the electron/hole has been scattered into a hybridized state, i.e. into a superposition between both layers, there is a non-zero probability of further scattering into the opposite layer.

Following the relaxation cascade, we can track the population transfer from the hybridised K<sub>W</sub>Λ<sub>hyb</sub><sup>(l)</sup> to the interlayer K<sub>W</sub>K<sub>Mo</sub><sup>(l)</sup> excitons (solid and dashed blue lines in Fig. 3). After 100 fs, the initially populated intralayer K<sub>W</sub>K<sub>W</sub> exciton states has been almost completely emptied and most occupation is found in the interlayer K<sub>W</sub>K<sub>Mo</sub><sup>(l)</sup> excitons, where electrons and holes are spatially separated. As a result, the transfer of electrons from the initial WSe<sub>2</sub> layer into the opposite MoSe<sub>2</sub> layer occurs on sub-100fs timescale.

To further illustrate the main scattering processes governing the relaxation cascade, Fig. 4 shows the momentum-resolved exciton dynamics for different times. We find that in the first step the hybridised K<sub>W</sub>Λ<sub>hyb</sub> and K<sub>W</sub>Λ<sub>hyb</sub><sup>(l)</sup> states are not populated (0 fs). The scattering into the latter happens on a faster timescale, as here M phonons are involved which are known to give rise to a

very efficient scattering with excitons [45]. With some delay, there is an efficient phonon-mediated scattering from these hybridized states into the interlayer  $K_W K_{Mo}$  and  $K_W K'_{Mo}$  excitons. The population of the latter occurs faster again due to the involved M phonons. In the final step, this state becomes partially depopulated in favor of the energetically lowest  $K_W K_{Mo}$  state. After approximately 500 fs a thermalized exciton distribution is reached with the highest occupation in  $K_W K_{Mo}$  followed by a certain thermal occupation in  $K_W K'_{Mo}$ . All other states have only a negligible population.

So far, we have investigated the simplified situation of an initially populated  $K_W K_W$ . In a real experiment, this state will be continuously optically excited throughout a finite time window and there will be an interplay of excitation and phonon-mediated scattering. Evaluating Eq. (3) we can resolve this interplay and find the same general behavior as described above, cf. the SI. We observe the same main relaxation steps and a very similar timescale for the charge transfer mechanism. However, tracking the dynamics becomes more complicated during the initial phase of the relaxation due to the simultaneous pumping of excitons in the system that immediately start to relax very rapidly. The main difference between the simulation with a pump pulse (Fig. 3 SI) and the instantaneous initialization is that at the time when the laser pulse reaches its maximum a large fraction of excitons has already relaxed to lower energy states, which quantitatively modifies the delay between peak populations of hybrid and interlayer exciton states. This suggests that we can capture the main features of the process using instantaneous excitation which allows us to gain a much more intuitive picture of the charge transfer without losing generality.

## INTERLAYER CHARGE TRANSFER

Summarizing the exciton dynamics in a nutshell, the initially inserted occupation of the intralayer  $K_W K_W$  excitons is distributed to the energetically lowest interlayer  $K_W K_{Mo}^{(l)}$  states through an intermediate step involving strongly hybridized  $K\Lambda/\Lambda^{(l)}$  states. This means that the charge transfer is a two-step process, where the electron is first transferred into a hybrid state (representing a superposition of both layers) and in a second step it is transferred to the opposite layer. The characteristic charge transfer time  $\tau$  is illustrated in Fig. 5(a) as a function of temperature for different high-symmetry stackings. We can quantify the charge transfer speed by computing the layer- and stacking-dependent probability  $P_e(t) = \langle a_c^\dagger a_c \rangle$  of one electron being localized in the MoSe<sub>2</sub> layer after excitation of an intralayer state in the WSe<sub>2</sub> layer, cf. Fig. 5(b). By exponentially fitting the temporal evolution of  $P_e(t)$ , we can extract the characteristic electron transfer time  $\tau$ . We find an ultrafast transfer rate of  $\tau = 33$  fs for

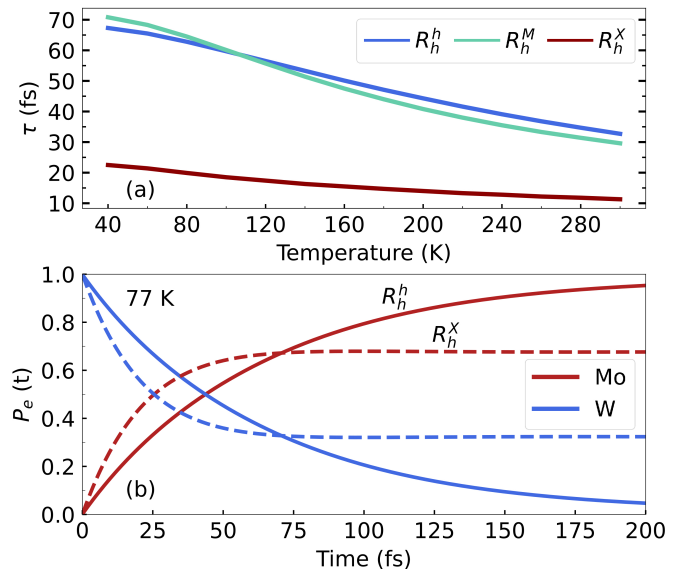


FIG. 5. (a) Characteristic electron transfer time as a function of temperature for MoSe<sub>2</sub>-WSe<sub>2</sub> in different high-symmetry stackings. The time is extracted from an exponential fit of the layer-dependent electron probability  $P_e(t)$  as shown in part (b). We find a considerable decrease in the charge transfer time with temperature reflecting a more efficient exciton-phonon scattering. Interestingly, we predict a much faster transfer time for  $R_h^X$  stacking, as here the hybrid  $\Lambda_{hyb}^{(l)}$  states are very close to the interlayer  $K_W K_{Mo}^{(l)}$  states, cf the SI. The faster electron transfer speed comes at the cost of a more incomplete transfer process as the stationary occupation of the  $\Lambda_{hyb}^{(l)}$  excitons is relatively high, where the electrons is delocalized between both layers, cf. the dashed vs solid lines in part b.

MoSe<sub>2</sub>-WSe<sub>2</sub> in  $R_h^h$  stacking at room temperature. The electrons are almost completely transferred from the initially occupied WSe<sub>2</sub> layer to the MoSe<sub>2</sub> layer, i.e. one finds the electron with a probability of 95% after 200 fs, cf. the solid red and blue lines in Fig. 5(b).

Since the relaxation cascade is mediated by phonons, we find a pronounced temperature dependence of the transfer time. Concretely, we predict an increase in  $\tau(T)$  by approximately a factor of 2 to  $\tau = 67$  fs at 40 K for  $R_h^h$  stacking. The reason is the reduced scattering efficiency with phonons at lower temperatures. Nevertheless, even at cryogenic temperatures we find an ultrafast charge transfer as the relaxation cascade occurs toward energetically lower exciton states and is driven by phonon emission.

Interestingly, we find an unexpected acceleration of the charge transfer for  $R_h^X$  stacking (whereas  $R_h^M$  stacking is rather similar to the  $R_h^h$  stacking investigated so far). This originates from the hybrid-energy landscape for different stackings (cf. the SI). The stronger tunnelling at the KA valley for the  $R_h^X$  stacking [27] and the resulting larger red-shift of exciton energies has as a conse-

quence that the relevant energy levels are closer than in other stackings, cf. Fig. 2(a) in the SI. In particular, the strongly hybridised  $\text{KA}_{\text{hyb}}$  states and the interlayer  $\text{K}_\text{W}\text{K}_{\text{Mo}}^{(\prime)}$  excitons are nearly degenerate. As a result, the second step in the charge transfer process is much more efficient compared to the  $\text{R}_h^h$  stacking. Note however that while the charge transfer is indeed faster for the  $\text{R}_h^X$  stacking, there is only an incomplete transfer. This means that the electron is not transferred to almost 100% as in the case of  $\text{R}_h^h$  stacking, but there is still a probability of approximately 40% to find the electron in the initially populated layer, cf. the dashed lines in Fig. 5(b). The reason behind this is that a large percentage of the hybrid-exciton population remains in the hybrid  $\text{KA}_{\text{hyb}}$  state as it is threefold degenerate and very close in energy with the lowest interlayer  $\text{K}_\text{W}\text{K}_{\text{Mo}}$  state. Hence, the electron remains partially delocalized between the two layers and the charge transfer is incomplete.

So far we have investigated the  $\text{MoSe}_2$ - $\text{WSe}_2$  heterostructure. The comparison with  $\text{MoS}_2$ - $\text{WS}_2$  (shown in the SI) yields the same general behavior for the hybrid-exciton relaxation dynamics. We find a somewhat slower charge transfer with  $\tau = 88$  fs for  $\text{R}_h^h$  stacking at room temperature, mainly due to the much larger energy window involved in the relaxation dynamics, cf. the energy landscape in Fig. S4 in the SI. Analyzing the results in more detail, we find the main difference originating from the importance of  $\Gamma_{\text{hyb}}\text{K}$  excitons. The strong tunnelling occurring in the  $\Gamma$  valley results in a large red-shift of the corresponding exciton states making them energetically lowest in  $\text{MoS}_2$ - $\text{WS}_2$ . Interestingly, we find that in contrast to  $\text{MoSe}_2$ - $\text{WSe}_2$  discussed above, we find here the slowest charge transfer for the  $\text{R}_h^X$  stacking. This can be traced back to  $\Gamma_{\text{hyb}}\text{K}_\text{W}$  states which trap excitons as the only states that are close in energy and have a similar composition are  $\text{KA}_{\text{hyb}}^{(\prime)}$  excitons. However, scattering into the latter from  $\Gamma_{\text{hyb}}\text{K}_\text{W}$  requires a simultaneous electron and hole transfer and is thus a negligible higher-order process. A more detailed description of the relaxation dynamics as well as temperature- and stacking-dependent charge transfer times in the  $\text{MoS}_2$ - $\text{WS}_2$  heterostructure can be found in the SI.

In conclusion, we have developed a microscopic and material-specific theory allowing us to access the relaxation dynamics of hybrid excitons in van der Waals heterostructures. In particular, we identify the extremely efficient phonon-mediated relaxation via strongly hybridized  $\text{KA}_{\text{hyb}}$  excitons as the crucial mechanism behind the ultrafast charge transfer process in the  $\text{MoSe}_2$ - $\text{WSe}_2$  heterostructure. We predict charge transfer times in the range of tens of femtoseconds that are strongly dependent on temperature and stacking of the layers. Our work presents an important step towards a microscopic understanding of the relaxation cascade and ultrafast charge transfer in technologically

promising van der Waals heterostructures.

We acknowledge support from Deutsche Forschungsgemeinschaft (DFG) via SFB 1083 (Project B9) and the European Unions Horizon 2020 Research and Innovation Program, under Grant Agreement No. 881603 (Graphene Flagship).

#### DATA AVAILABILITY STATEMENT

The data that support the findings of this study are available from the corresponding author upon reasonable request.

#### CONFLICT OF INTEREST

The authors declare no conflict of interest

---

\* giuseppe.meneghini@physik.uni-marburg.de

- [1] Keliang He, Nardeep Kumar, Liang Zhao, Zefang Wang, Kin Fai Mak, Hui Zhao, and Jie Shan, “Tightly bound excitons in monolayer  $\text{WSe}_2$ ,” *Physical Review Letters* **113**, 026803 (2014).
- [2] Alexey Chernikov, Timothy C Berkelbach, Heather M Hill, Albert Rigosi, Yilei Li, Ozgur Burak Aslan, David R Reichman, Mark S Hybertsen, and Tony F Heinz, “Exciton binding energy and nonhydrogenic rydberg series in monolayer  $\text{WS}_2$ ,” *Physical Review Letters* **113**, 076802 (2014).
- [3] Gang Wang, Alexey Chernikov, Mikhail M Glazov, Tony F Heinz, Xavier Marie, Thierry Amand, and Bernhard Urbaszek, “Colloquium: Excitons in atomically thin transition metal dichalcogenides,” *Reviews of Modern Physics* **90**, 021001 (2018).
- [4] Thomas Mueller and Ermin Malic, “Exciton physics and device application of two-dimensional transition metal dichalcogenide semiconductors,” *npj 2D Materials and Applications* **2**, 1–12 (2018).
- [5] Pasqual Rivera, John R Schaibley, Aaron M Jones, Jason S Ross, Sanfeng Wu, Grant Aivazian, Philip Klement, Kyle Seyler, Genevieve Clark, Nirmal J Ghimire, *et al.*, “Observation of long-lived interlayer excitons in monolayer  $\text{MoSe}_2$ - $\text{WSe}_2$  heterostructures,” *Nature Communications* **6**, 1–6 (2015).
- [6] Bastian Miller, Alexander Steinhoff, Borja Pano, Julian Klein, Frank Jahnke, Alexander Holleitner, and Ursula Wurstbauer, “Long-lived direct and indirect interlayer excitons in van der waals heterostructures,” *Nano Letters* **17**, 5229–5237 (2017).
- [7] Jens Kunstmann, Fabian Mooshammer, Philipp Nagler, Andrey Chaves, Frederick Stein, Nicola Paradiso, Gerd Plechinger, Christoph Strunk, Christian Schüller, Gotthard Seifert, *et al.*, “Momentum-space indirect interlayer excitons in transition-metal dichalcogenide van der waals heterostructures,” *Nature Physics* **14**, 801–805 (2018).
- [8] Chenhao Jin, Emma C Regan, Aiming Yan, M Iqbal Bakti Utama, Danqing Wang, Sihan Zhao, Ying Qin, Sijie Yang, Zhiren Zheng, Shenyang Shi, *et al.*, “Observation of moiré excitons in  $\text{WSe}_2/\text{WS}_2$  heterostructure superlattices,” *Nature* **567**, 76–80 (2019).
- [9] Kha Tran, Galan Moody, Fengcheng Wu, Xiaobo Lu,

- Junho Choi, Kyoungwan Kim, Amrithes Rai, Daniel A Sanchez, Jiamin Quan, Akshay Singh, *et al.*, “Evidence for moiré excitons in van der waals heterostructures,” *Nature* **567**, 71–75 (2019).
- [10] Kyle L Seyler, Pasqual Rivera, Hongyi Yu, Nathan P Wilson, Essance L Ray, David G Mandrus, Jiaqiang Yan, Wang Yao, and Xiaodong Xu, “Signatures of moiré-trapped valley excitons in MoSe<sub>2</sub>/WSe<sub>2</sub> heterobilayers,” *Nature* **567**, 66–70 (2019).
- [11] Evgeny M Alexeev, David A Ruiz-Tijerina, Mark Danovich, Matthew J Hamer, Daniel J Terry, Pramoda K Nayak, Seongjoon Ahn, Sangyeon Pak, Juwon Lee, Jung Inn Sohn, *et al.*, “Resonantly hybridized excitons in moiré superlattices in van der waals heterostructures,” *Nature* **567**, 81–86 (2019).
- [12] David A Ruiz-Tijerina and Vladimir I Fal’ko, “Interlayer hybridization and moiré superlattice minibands for electrons and excitons in heterobilayers of transition-metal dichalcogenides,” *Physical Review B* **99**, 125424 (2019).
- [13] Lukas Sigl, Mirco Troue, Manuel Katzer, Malte Selig, Florian Sigger, Jonas Kiemle, Mauro Brotons-Gisbert, Kenji Watanabe, Takashi Taniguchi, Brian D Gerardot, *et al.*, “Optical dipole orientation of interlayer excitons in mose 2- wse 2 heterostacks,” *Physical Review B* **105**, 035417 (2022).
- [14] Johannes Holler, Malte Selig, Michael Kempf, Jonas Zipfel, Philipp Nagler, Manuel Katzer, Florian Katsch, Mariana V Ballottin, Anatolie A Mitioglu, Alexey Chernikov, *et al.*, “Interlayer exciton valley polarization dynamics in large magnetic fields,” *Physical Review B* **105**, 085303 (2022).
- [15] Xiaoping Hong, Jonghwan Kim, Su-Fei Shi, Yu Zhang, Chenhao Jin, Yinghui Sun, Sefaattin Tongay, Junqiao Wu, Yanfeng Zhang, and Feng Wang, “Ultrafast charge transfer in atomically thin mos<sub>2</sub>/ws<sub>2</sub> heterostructures,” *Nature nanotechnology* **9**, 682–686 (2014).
- [16] Frank Ceballos, Matthew Z Bellus, Hsin-Ying Chiu, and Hui Zhao, “Ultrafast charge separation and indirect exciton formation in a mos<sub>2</sub>–mose<sub>2</sub> van der waals heterostructure,” *ACS nano* **8**, 12717–12724 (2014).
- [17] Ziheng Ji, Hao Hong, Jin Zhang, Qi Zhang, Wei Huang, Ting Cao, Ruixi Qiao, Can Liu, Jing Liang, Chuanhong Jin, *et al.*, “Robust stacking-independent ultrafast charge transfer in mos<sub>2</sub>/ws<sub>2</sub> bilayers,” *ACS nano* **11**, 12020–12026 (2017).
- [18] Philipp Merkl, Fabian Mooshammer, Philipp Steinleitner, Anna Girnghuber, K-Q Lin, Philipp Nagler, Johannes Holler, Christian Schüller, John M Lupton, Tobias Korn, *et al.*, “Ultrafast transition between exciton phases in van der waals heterostructures,” *Nature Materials* **18**, 691–696 (2019).
- [19] David Schmitt, Jan Philipp Bange, Wiebke Bennecke, AbdulAziz AlMutairi, Kenji Watanabe, Takashi Taniguchi, Daniel Steil, D Russell Luke, R Thomas Weitz, Sabine Steil, *et al.*, “Formation of moire interlayer excitons in space and time,” arXiv preprint arXiv:2112.05011 (2021).
- [20] Thorsten Deilmann and Kristian Sommer Thygesen, “Interlayer excitons with large optical amplitudes in layered van der waals materials,” *Nano Letters* **18**, 2984 (2018).
- [21] Heather M Hill, Albert F Rigosi, Kwang Taeg Rim, George W Flynn, and Tony F Heinz, “Band alignment in mos<sub>2</sub>/ws<sub>2</sub> transition metal dichalcogenide heterostructures probed by scanning tunneling microscopy and spectroscopy,” *Nano letters* **16**, 4831–4837 (2016).
- [22] V Ongun Özcelik, Javad G Azadani, Ce Yang, Steven J Koester, and Tony Low, “Band alignment of two-dimensional semiconductors for designing heterostructures with momentum space matching,” *Physical Review B* **94**, 035125 (2016).
- [23] Simon Ovesen, Samuel Brem, Christopher Linderälv, Mikael Kuisma, Tobias Korn, Paul Erhart, Malte Selig, and Ermin Malic, “Interlayer exciton dynamics in van der waals heterostructures,” *Communications Physics* **2**, 1–8 (2019).
- [24] Yong Wang, Zhan Wang, Wang Yao, Gui-Bin Liu, and Hongyi Yu, “Interlayer coupling in commensurate and incommensurate bilayer structures of transition-metal dichalcogenides,” *Physical Review B* **95**, 115429 (2017).
- [25] Qijing Zheng, Wissam A Saidi, Yu Xie, Zhenggang Lan, Oleg V Prezhdo, Hrvoje Petek, and Jin Zhao, “Phonon-assisted ultrafast charge transfer at van der waals heterostructure interface,” *Nano letters* **17**, 6435–6442 (2017).
- [26] Fang Liu, Qiuyang Li, and X-Y Zhu, “Direct determination of momentum-resolved electron transfer in the photoexcited van der waals heterobilayer w s 2/mo s 2,” *Physical Review B* **101**, 201405 (2020).
- [27] Joakim Hagel, Samuel Brem, Christopher Linderälv, Paul Erhart, and Ermin Malic, “Exciton landscape in van der waals heterostructures,” *Physical Review Research* **3**, 043217 (2021).
- [28] Samuel Brem, Christopher Linderälv, Paul Erhart, and Ermin Malic, “Tunable phases of moiré excitons in van der waals heterostructures,” *Nano letters* **20**, 8534–8540 (2020).
- [29] Florian Katsch, Malte Selig, Alexander Carmele, and Andreas Knorr, “Theory of exciton–exciton interactions in monolayer transition metal dichalcogenides,” *Physica Status Solidi (b)* **255**, 1800185 (2018).
- [30] Samuel Brem, Kai-Qiang Lin, Roland Gillen, Jonas M Bauer, Janina Maultzsch, John M Lupton, and Ermin Malic, “Hybridized intervalley moiré excitons and flat bands in twisted wse 2 bilayers,” *Nanoscale* **12**, 11088–11094 (2020).
- [31] Philipp Merkl, Fabian Mooshammer, Samuel Brem, Anna Girnghuber, Kai-Qiang Lin, Leonard Weigl, Marlene Liebich, Chaw-Keong Yong, Roland Gillen, Janina Maultzsch, *et al.*, “Twist-tailoring coulomb correlations in van der waals homobilayers,” *Nature Communications* **11**, 1–7 (2020).
- [32] Andor Kormányos, Guido Burkard, Martin Gmitra, Jaroslav Fabian, Viktor Zolyomi, Neil D Drummond, and Vladimir Fal’ko, “k-p theory for two-dimensional transition metal dichalcogenide semiconductors,” *2D Materials* **2**, 022001 (2015).
- [33] Akash Laturia, Maarten L Van de Put, and William G Vandenberghe, “Dielectric properties of hexagonal boron nitride and transition metal dichalcogenides: from monolayer to bulk,” *npj 2D Materials and Applications* **2**, 1–7 (2018).
- [34] Yang Song and Hanan Dery, “Transport theory of monolayer transition-metal dichalcogenides through symmetry,” *Physical review letters* **111**, 026601 (2013).
- [35] Mikhail M Glazov, Thierry Amand, Xavier Marie, Delphine Lagarde, Louis Bouet, and Bernhard Urbaszek, “Exciton fine structure and spin decoherence in monolayers of transition metal dichalcogenides,” *Physical Review*

- B **89**, 201302 (2014).
- [36] Malte Selig, Gunnar Berghäuser, Marten Richter, Rudolf Bratschitsch, Andreas Knorr, and Ermin Malic, “Dark and bright exciton formation, thermalization, and photoluminescence in monolayer transition metal dichalcogenides,” *2D Materials* **5**, 035017 (2018).
- [37] Thorsten Deilmann and Kristian Sommer Thygesen, “Finite-momentum exciton landscape in mono- and bilayer transition metal dichalcogenides,” *2D Materials* **6**, 035003 (2019).
- [38] D. Erckensten, S. Brem, K. Wagner, R. Gillen, R. Perea-Causin, J. D. Ziegler, T. Taniguchi, K. Watanabe, J. Maultzsch, and A. Chernikov und E. Malic, “Dark exciton-exciton annihilation in monolayer transition-metal dichalcogenides,” *Phys. Rev. B* **104**, L241406 (2021).
- [39] Hartmut Haug and Stephan W Koch, *Quantum theory of the optical and electronic properties of semiconductors* (World Scientific Publishing Company, 2009).
- [40] A Thränhardt, S Kuckenbug, A Knorr, T Meier, and SW Koch, “Quantum theory of phonon-assisted exciton formation and luminescence in semiconductor quantum wells,” *Physical Review B* **62**, 2706 (2000).
- [41] Samuel Brem, Malte Selig, Gunnar Berghäuser, and Ermin Malic, “Exciton relaxation cascade in two-dimensional transition metal dichalcogenides,” *Scientific reports* **8**, 1–8 (2018).
- [42] E Cappelluti, Rafael Roldán, JA Silva-Guillén, Pablo Ordejón, and F Guinea, “Tight-binding model and direct-gap/indirect-gap transition in single-layer and multilayers 2,” *Physical Review B* **88**, 075409 (2013).
- [43] Roland Gillen and Janina Maultzsch, “Interlayer excitons in MoSe<sub>2</sub>/WSe<sub>2</sub> heterostructures from first principles,” *Physical Review B* **97**, 165306 (2018).
- [44] Samuel Brem, Jonas Zipfel, Malte Selig, Archana Raja, Lutz Waldecker, Jonas D Ziegler, Takashi Taniguchi, Kenji Watanabe, Alexey Chernikov, and Ermin Malic, “Intrinsic lifetime of higher excitonic states in tungsten diselenide monolayers,” *Nanoscale* **11**, 12381–12387 (2019).
- [45] Jin Z, Li X, Mullen J T, and Kim K W, “Intrinsic transport properties of electrons and holes in monolayer transition-metal dichalcogenides,” *Phys. Rev. B* **90**, 045422 (2014).